Available on the CERN CDS information server **CMS PAS SUS-16-047**

CMS Physics Analysis Summary

Contact: cms-pag-conveners-susy@cern.ch 2017/03/23

Search for supersymmetry in events with at least one photon, missing transverse momentum, and large transverse event activity in proton-proton collisions at 13 TeV

The CMS Collaboration

Abstract

A search for physics beyond the standard model in final states with at least one photon, large transverse momentum imbalance, and large total transverse event activity is presented. This event selection provides good sensitivity for gauge mediated supersymmetry models in which pair-produced gluinos or squarks decay via short-living neutralinos to photons and gravitinos. The data sample corresponds to an integrated luminosity of 35.9 fb^{-1} of proton-proton collisions recorded by the CMS experiment at the LHC in 2016. No excess of events above the standard model background is observed. The data is interpreted in simplified models of gluino- and squark pair production, in which gluinos and squarks decay via gauginos to photons. Gluino masses of up to 2 TeV masses up to 1.6 TeV are excluded.

1 Introduction

The standard model (SM) of particle physics describes elementary particles and their interactions successfully. Nevertheless, fine tuning of SM parameters is needed to cancel large quantum corrections to the mass term in the Higgs potential [1]. This and other problems of the SM are addressed by supersymmetry (SUSY) [2–8], in which a supersymmetric partner particle is predicted for each SM particle. Gauge mediated SUSY breaking (GMSB) [9–15] models also allow for a natural suppression of flavour violations in the supersymmetric sector and can give rise to interesting phenomena [16].

R-parity [17, 18] conservation implies that SUSY particles are produced in pairs and the lightest supersymmetric particle (LSP) is stable. If the LSP is neutral, it can leave the detector unobserved and leading to an imbalance of the total transverse momentum. In this analysis, R-parity conservation is assumed and the lightest supersymmetric particle is assumed to be a near massless gravitino $\widetilde{\mathrm{G}}$. The next-to-lightest SUSY particle is assumed to be a gaugino $\widetilde{\chi}_1^{0/\pm}$, which decays to a SM boson and a gravitino. Both bino- and wino-like neutralinos $\widetilde{\chi}_1^0$ can decay to a photon and a gravitino; wino-like charginos $\widetilde{\chi}_1^{\pm}$ decay typically to a W boson and a gravitino. If the gauginos are produced in decay chains of primary squark and gluinos, the events also contain jets.

In this note, a search for physics beyond the standard model (BSM) in final states with at least one photon, large transverse momentum imbalance, and large total transverse event activity is reported. Similar searches have been performed by CMS at lower centre-of-mass energies [19], by the ATLAS collaboration [20, 21], and with alternative selections [22, 23]. No signs for BSM physics have yet been found, but additional BSM phase space can be probed with the data presented in this note corresponding to an integrated luminosity of 35.9 fb^{-1} of proton-proton collisions at 13 TeV center-of-mass energy.

This note is structured as follows. Section 2 describes the CMS detector. Event reconstruction and simulation are described in Section 3. In Section 4, the search strategy and background estimation are discussed. Section 5 presents the results, which are interpreted in Section 6.

2 The CMS detector

The central feature of the CMS apparatus is a superconducting solenoid of 6 m internal diameter, providing a magnetic field of 3.8 T. Within the solenoid volume are a silicon pixel and strip tracker, a lead tungstate crystal electromagnetic calorimeter (ECAL), and a brass and scintillator hadron calorimeter (HCAL), each composed of a barrel and two endcap sections. The electromagnetic calorimeter consists of 75 848 lead tungstate crystals, which provide coverage in pseudorapidity $|\eta| < 1.48$ in a barrel region (EB) and $1.48 < |\eta| < 3.0$ in two endcap regions (EE). Forward calorimeters extend the pseudorapidity coverage provided by the barrel and endcap detectors. Muons are measured in gas-ionization detectors embedded in the steel flux-return yoke outside the solenoid.

In the barrel section of the ECAL, an energy resolution of about 1% is achieved for unconverted or late-converting photons in the tens of GeV energy range. The remaining barrel photons have a resolution of about 1.3% up to a pseudorapidity of $|\eta| = 1$, rising to about 2.5% at $|\eta| = 1.4$ [24]. The jet energy resolution amounts typically to 15% at 10 GeV, 8% at 100 GeV, and 4% at 1 TeV, when combining information from the entire detector [25].

A more detailed description of the CMS detector, together with a definition of the coordinate system used and the relevant kinematic variables, can be found in Ref. [26].

3 Event reconstruction and simulation

The particle-flow (PF) event algorithm reconstructs and identifies each individual particle with an optimized combination of information from the various elements of the CMS detector [27, 28]. The energy of photons is directly obtained from the ECAL measurement. The energy of electrons is determined from a combination of the electron momentum at the primary interaction vertex as measured by the tracker, the energy of the corresponding ECAL cluster, and the energy sum of all bremsstrahlung photons spatially compatible with originating from the electron track. The momentum of muons is obtained from the curvature of the corresponding track. The energy of charged hadrons is determined from a combination of their momentum measured in the tracker and the matching ECAL and HCAL energy deposits, corrected for zero-suppression effects and for the response function of the calorimeters to hadronic showers. Finally, the energy of neutral hadrons is obtained from the corresponding corrected ECAL and HCAL energy.

Jets are reconstructed from all PF candidates, clustered by the anti-k_t algorithm [29, 30] with a size parameter of 0.4. Charged particles from additional proton-proton collisions from the same or adjacent beam crossing as the primary hard-scattering process ("pileup") are excluded if they do not originate from the interaction vertex with the largest sum of transverse momenta, calculated from all its associated tracks.

The jet momentum is determined as the vectorial sum of all particle momenta in the jet, and is found from simulation to be within 5 to 10% of the true momentum over the whole p_T spectrum and detector acceptance. An offset correction is applied to jet energies to take into account the contribution from additional proton-proton interactions within the same or nearby bunch crossings. Jet energy corrections are derived from simulation, and are confirmed with in situ measurements of the energy balance in dijet and γ + jet events. Additional selection criteria are applied to remove events with spurious signals from instrumental noise.

The missing transverse momentum $\vec{p}_T^{\,miss}$ is defined as the negative of the vector sum of the transverse momenta p_T of all PF candidates in the event, and its magnitude is denoted by p_T^{miss}. The total transverse energy EMH_T is the scalar sum of all jet p_T for jets with $p_T > 30\,GeV$ and $|\eta| < 3$. If a jet overlaps with a photon in an angular distance $\Delta R < 0.4$, the p_T of the photon is added to EMH_T instead of the jet.

Monte Carlo generated events are used to study the SM backgrounds, develop and validate the background estimation techniques and model signal scenarios. The MADGRAPH MC@NLO 2.2.2 [31] generator is used to generate γ + jet, multijet, Z, W, γW, γZ, gluino-pair, and squark-pair events in leading order mode, while the next-to-leading order mode of MADGRAPH MC@NLO is used for $\gamma t\bar{t}$ events. The NNPDF3.0 [32] parton distribution functions (PDF) are used in conjunction with PYTHIA 8 [33] for simulating the showering and hadronization. Leading order cross sections are used for γ + jet events and events comprised uniquely of jets produced through the strong interaction (multijet events). Next-to-leading order (NLO) cross sections are used for all for other processes.

Gluino- and squark-pair production cross sections are determined using NLO plus next-to-leading-logarithm (NLL) calculations [34]. Four simplified models [35] are considered: T6gg, where a first- or second-generation squark and an anti-squark are produced, and each decays to a quark and a neutralino. The neutralino decays further promptly to a photon and a gravitino, resulting in a final state with two jets, two photons and two gravitinos. T6Wg is similar, except that 50% of the squarks decay to a quark and a neutralino, while 50% of the squarks decay to a chargino and a quark. The chargino further decays to a W boson and a gravitino, resulting in

final states with at least two jets, two gravitinos and either two photons, one photon and one W boson, or two W bosons. T5gg and T5Wg consist of gluino-pair production. For these models, the squark mass is assumed to be much larger than the gluino mass, leading to a three-body decay of the gluino to two jets and a gaugino. For T5gg, the gauginos are neutralinos, while for T5Wg, the gluino can also decay to jets and a chargino. Branching fractions are assumed to be 100%, except the squark to neutralino decay in the T6Wg and the gluino to neutralino decay in the T5Wg model, which is 50%. Feynman diagrams of the processes are shown in Fig. 1.

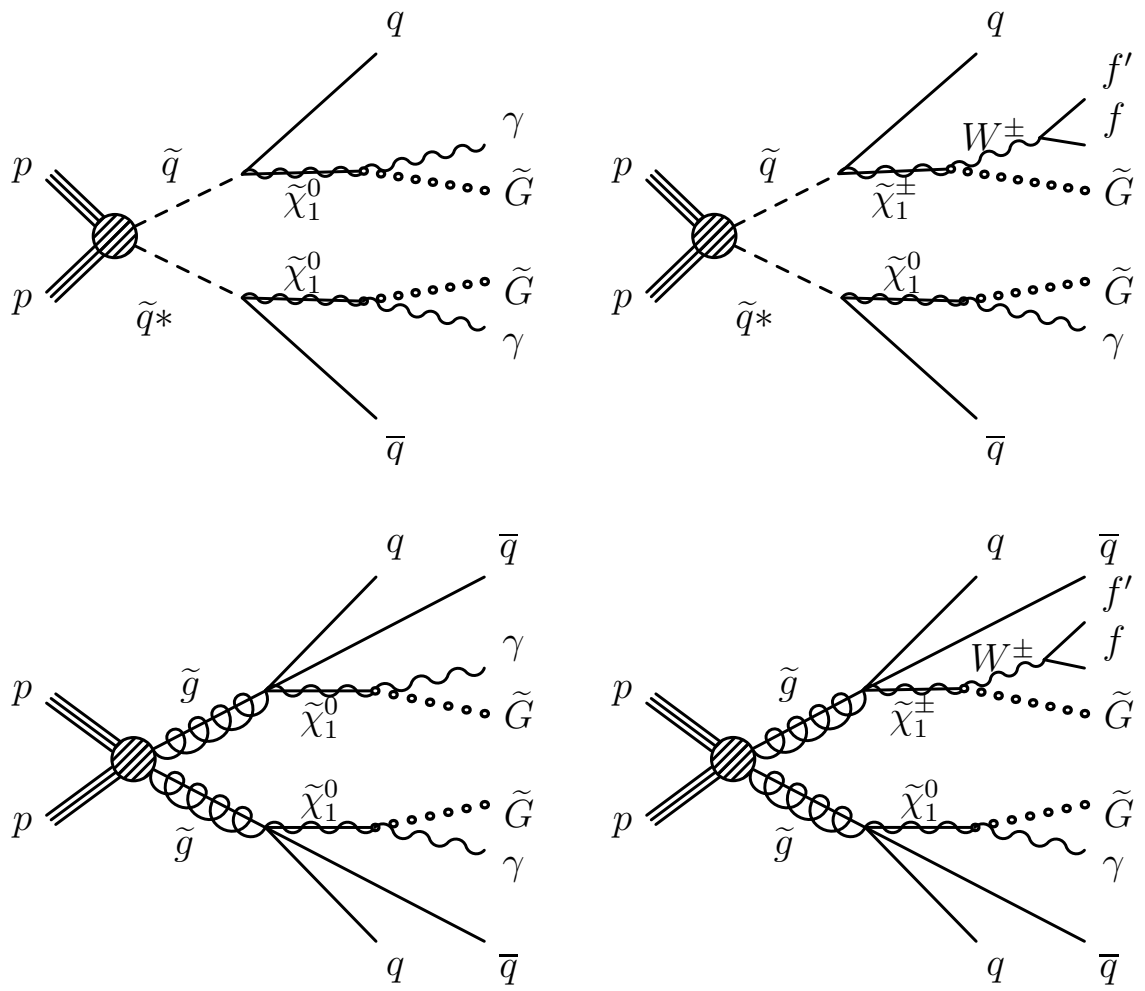

Figure 1: Feynman diagrams for simulated signal processes: T6gg (top left), T6Wg (top right), T5gg (bottom left) and T5Wg (bottom right).

The CMS detector response is simulated using GEANT4 [36] for SM processes, while for signal events we use the CMS fast simulation [37]. Event reconstruction is performed in the same manner as for collision data.

4 Event selection and search strategy

In the first trigger stage, events with an electromagnetic cluster are selected. The high-level-trigger system selects events containing at least one photon with $p_{\mathrm{T}} > 90\,\mathrm{GeV}$ and $|\eta| < 2.5$, and $H_{\mathrm{T}} > 600\,\mathrm{GeV}$, where H_{T} is defined as the scalar sum of the p_{T} for all jets passing the

selection used to calculate EMH_T. The trigger does not distinguish between jets and photons, so that photons reconstructed as jets are included.

Events are selected if they contain at least one photon with $p_T > 100\,\text{GeV}$ in the EB with $|\eta| < 1.4442$. To reliably predict the background, the photon is not allowed to be parallel or anti-parallel to $\vec{p}_T^{\,\text{miss}}$ within an azimuthal angle of $\left|\Delta\Phi(\pm\vec{p}_T^{\,\text{miss}}, \vec{p}_T^{\,\gamma})\right| < 0.3$. Three high p_T^{miss} ranges (350–450 GeV, 450–600 GeV, and $\geq 600\,\text{GeV}$) and two EMH_T selections (700–2000 GeV and $\geq$ 2000 GeV) allow the definition of six search regions. Contributions of multijet, $\gamma +$ jet, γZ, γW, $\gamma t\bar{t}$, and events with electrons are estimated as described below.

4.1 Background contribution of events with non-genuine p_T^{miss}

$\gamma +$ jet events can contribute to the signal region due to the limited resolution of the detector. Jets have the largest momentum uncertainties, and even though the probability of a large mismeasurement is low, the large cross sections of this processes leads to a non-negligible contribution to the search region.

Multijet events have an even higher cross section, and contribute to the signal selection if additionally one of the jets is a misidentified as a photon. Non-zero p_T^{miss} in multijet events is also due to the jet momentum resolution.

Estimating these backgrounds from simulation would result in a large uncertainty for two reasons: the large cross section requires a large number of simulated events to obtain a small statistical uncertainty; In addition, small differences in the measured and simulated jet response can lead to large effects for large values of p_T^{miss}. A data-driven background estimation method can achieve smaller uncertainties without relying on the simulated jet energy response. In this note, it is performed in the low- and high-EMH_T selection independently. The shapes of the p_T^{miss} distributions in $\gamma +$ jet and multijet events are similar, and their normalizations can be extracted from low p_T^{miss} events, where no significant signal contribution is expected to be present. We use the shape of the p_T^{miss} distribution of a multijet event sample as a prediction for events with non-genuine p_T^{miss}.

For the background estimate, the photon-event selection is defined by requiring the search selection, but omitting the p_T^{miss} requirement. The jet-event selection is made by selecting events with the EMH_T criteria only. For these events, a trigger with only the H_T selection is used. For low p_T^{miss}, the jet-event selection is dominated by multijet events, but for high p_T^{miss}, also $W(\ell\nu)$+jet, $Z(\nu\nu)$+jet, and $t\bar{t}$ events can contribute, so they are subtracted based on simulation. The shape of the p_T^{miss} distribution of $\gamma +$ jet and multijet events in the photon-event selection is very similar to the shape of the p_T^{miss} distribution of the jet-event selection.

To improve the agreement between the photon- and jet-event selections, and to correct for residual effects, the p_T^{miss} of the jet-event selection is shifted by multiplying p_T^{miss} by a factor. This factor is chosen such that it minimizes the χ^2 between the shape of the p_T^{miss} distribution of the photon- and jet-event selection for $p_T^{\text{miss}} < 100\,\text{GeV}$. This deviation of the shift from unity is taken as systematic uncertainty. The p_T^{miss} distribution of the jet-event selection is then scaled to the p_T^{miss} distribution of the photon-event selection $p_T^{\text{miss}} < 100\,\text{GeV}$ and provides an estimate for the background of non-genuine p_T^{miss} events in the signal selection. The statistical uncertainty due to the χ^2 method is propagated to the prediction as well. We consider two sources of uncertainties for the background prediction: the uncertainty of the shift is propagated to the prediction as a shape uncertainty; second, the statistical uncertainty of the normalization in $p_T^{\text{miss}} < 100\,\text{GeV}$ is propagated as a systematic uncertainty. The statistical uncertainty assigned to the prediction due to the number of events in the jet-event selection with high p_T^{miss} is about

as large as the systematic uncertainty.

The method is tested on simulated γ + jet and multijet events. The direct simulation and the prediction from simulation, using this method, are shown in Fig. 2. In this and following figures, the last bin includes all events with $p_{\mathrm{T}}^{\mathrm{miss}} > 600\,\mathrm{GeV}$. The good agreement between the two distributions suggests the method is performing as expected. Further validation is discussed in Section 4.4.

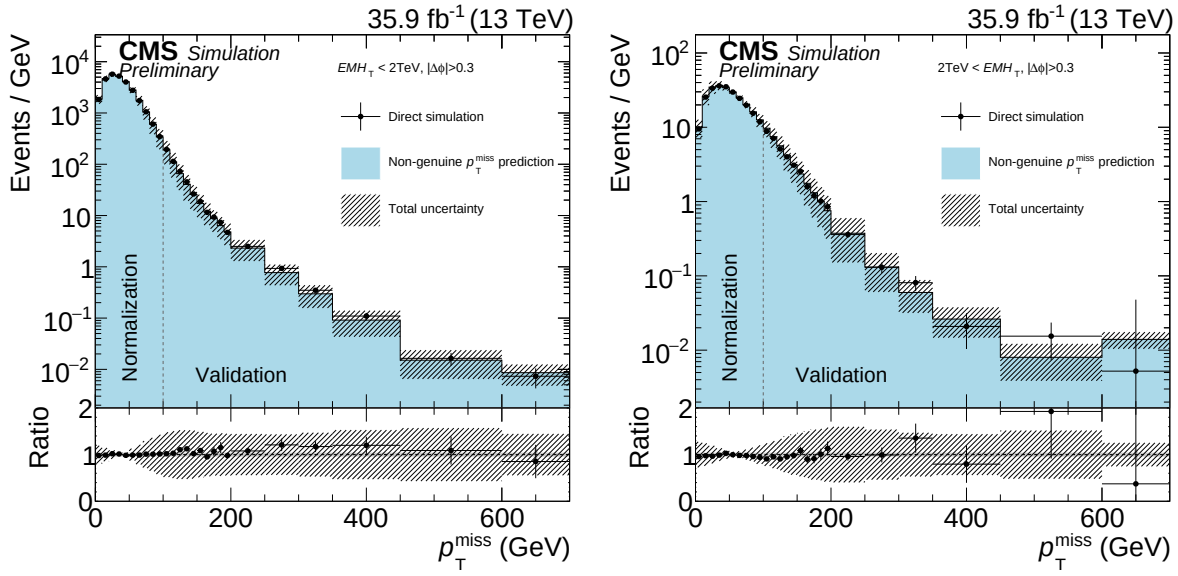

Figure 2: Validation of the non-genuine $p_{\mathrm{T}}^{\mathrm{miss}}$ background estimation method with γ + jet and multijet simulations. The low-EMH_{T} selection is shown on the left, the high-EMH_{T} selection on the right.

4.2 Background contribution of events with electrons

Electrons and photons have similar calorimetric response. To distinguish photons from electrons, photon candidates are not allowed to have pixel seeds. Pixel seeds are two or three hits in the pixel detector corresponding to the hypothetical trajectory from the proton-proton interaction point to the energy cluster in the ECAL, taking into account positively and negatively charged electron hypotheses. If no pixel seeds are reconstructed for an electron, it can be identified as a photon. In W or $\mathrm{t\bar{t}}$ processes, electrons are produced in association with neutrinos, so these events tend to also have large $p_{\mathrm{T}}^{\mathrm{miss}}$ and enter the search regions. To estimate the contribution of these processes, a control region with electrons is defined and scaled by the electron-to-photon misreconstruction probability.

The electron control selections are defined exactly as the photon selections, except that pixel seeds are required for the photon identification. For high $p_{\mathrm{T}}^{\mathrm{miss}}$, this selection is dominated by W and $\mathrm{t\bar{t}}$ events.

The electron-to-photon misreconstruction probability is estimated using an event sample dominated by Z$\rightarrow$ ee events, and is 2.7% for data and 1.5% for simulation. To account for differences in the misreconstruction rate on the Z-boson resonance and the W boson dominated signal region with high $p_{\mathrm{T}}^{\mathrm{miss}}$ and high EMH_{T}, a systematic uncertainty of 30% is applied to the misreconstruction rate.

The method is tested on simulated W+jet and $\mathrm{t\bar{t}}$ events. The direct simulation of electrons reconstructed as photons is compared to the electron control region, scaled by the electron-to-

photon misreconstruction probability as shown in Fig. 3. The agreement in the search regions suggest that the method is performing as expected.

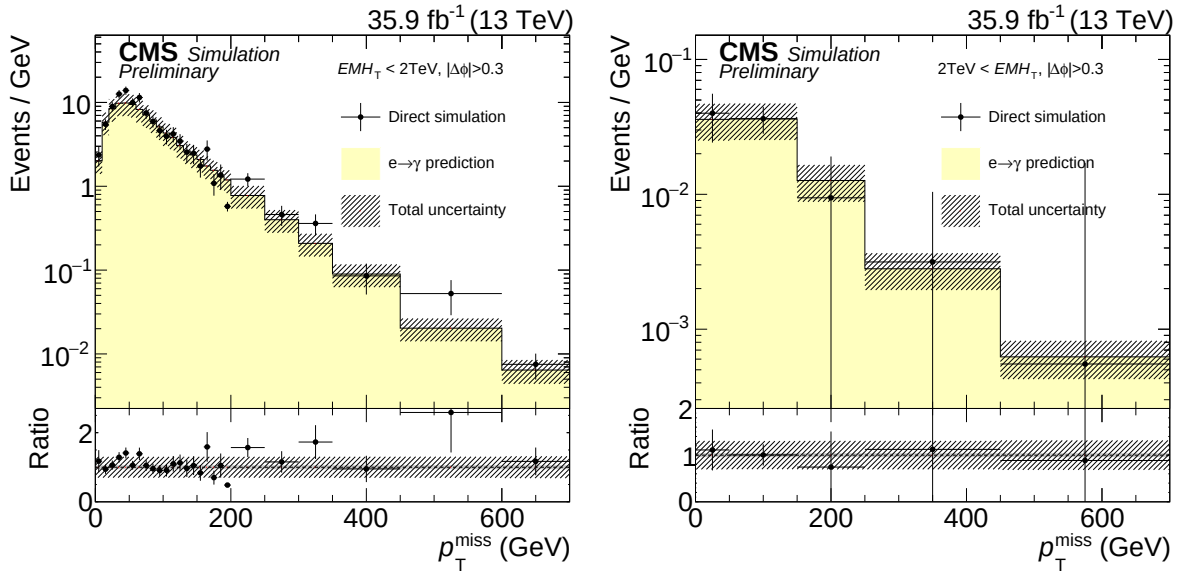

Figure 3: Validation of the background estimation method for electrons misreconstructed as photons, using W and $\mathrm{t\bar{t}}$ simulation. The low-(high-)EMH_{T} selection is shown on the left (right).

4.3 Directly simulated backgrounds

Also contributing to the search region are the processes $\gamma\mathrm{W}(\ell\nu)$, $\gamma\mathrm{Z}(\nu\nu)$, and $\gamma\mathrm{t\bar{t}}$, which are estimated using simulation. Simulated events with electrons reconstructed as photons are omitted since they are estimated using data. The photon in the event can be produced in the hard scattering or in the shower, either as initial state radiation, final state radiation or as a jet misreconstructed as a photon. Events are simulated with and without a photon in the hard scattering process, and the overlap between the samples is removed. Differences in the selection efficiencies between data and simulation are considered. NLO cross sections are used, and several uncertainties are considered: factorization and renormalization scale, contribution of pileup events, trigger efficiency, jet resolution, photon and jet energy scale, and statistical uncertainty.

4.4 Validation of the methods

The methods are also validated using data from two orthogonal event selections.

The first validation region is defined with non-central photons. Instead of the photon being reconstructed in the EB, the leading photon must be reconstructed in $1.6 < |\eta| < 2.5$. This is not the full range of the EE, but in this range the background contribution from electrons reconstructed as photons is similar to the one in the barrel search region. High mass gluinos and squarks tend to decay more centrally, leaving the endcap validation region essentially free of potential signal events. The same methods as for the barrel search regions are applied, and the resulting distributions are shown in Fig. 4. The $p_{\mathrm{T}}^{\mathrm{miss}}$ distributions of two signal models are added to the background prediction. In the low EMH_{T} region and for large $p_{\mathrm{T}}^{\mathrm{miss}}$ of the high EMH_{T} region, the observed number of events agrees with the prediction.

The second validation region is the region $100\,\mathrm{GeV} < p_{\mathrm{T}}^{\mathrm{miss}} < 350\,\mathrm{GeV}$, which is orthogonal to both the region used to normalize the multijet background ($p_{\mathrm{T}}^{\mathrm{miss}} < 100\,\mathrm{GeV}$) as well as the signal regions ($p_{\mathrm{T}}^{\mathrm{miss}} > 350\,\mathrm{GeV}$), and is shown in Fig. 5. Good agreement is observed as well.

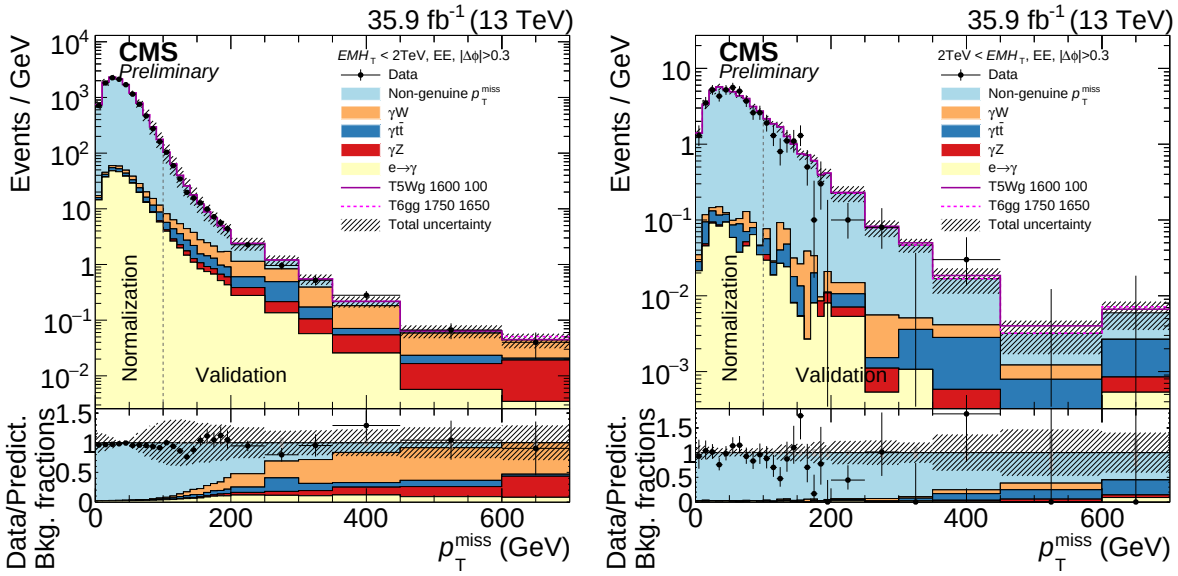

Figure 4: Validation of the background estimation methods with photons reconsructed in the endcap. The expectation for the T5Wg signal scenario with a gluino mass of 1600 GeV and a gaugino mass of 100 GeV and the T6gg signal scenario with a squark mass of 1750 GeV and a neutralino mass of 1650 GeV are shown added to the background. The low-(high-)EMH_T selection is shown on the left (right). Below the p_T^{miss} distributions, the data divided by the background prediction are shown as black dots, and the relative background components are shown as colored areas.

5 Results

The predicted number of SM background events and the number of observed events in data is shown in Fig. 5 and Table 1. In Fig. 5, the p_T^{miss} distributions of two signal models are added to the background prediction.

The low EMH_T search regions are dominated by γW events and are sensitive to signal models with low squark or gluino masses. The high EMH_T search regions are dominated by background with non genuine p_T^{miss} and have larger sensitivity to models with high gluino or squark masses and low gaugino masses. In total, the number of observed data events are in agreement with the prediction. The second search bin in both the low and high EMH_T region has an excess of about two standard deviations (s.d.). In the next higher bin in p_T^{miss}, which is more sensitive for most signal scenarios, the number of observed events is compatible with the background expectation.

6 Uncertainties and interpretation

The systematic uncertainties of the non-genuine p_T^{miss} background is fully correlated within the high- and low-EMH_T selections, and are described in Section 4.1. The systematic uncertainty on the electron misidentification background is fully correlated for all search regions, as are most uncertainties for the simulated backgrounds. The renormalization, factorization and PDF uncertainties on the cross sections for signal simulation are taken from [34]. The pileup uncertainty corresponds to a shift of the total inelastic proton-proton cross section by $\pm 5\%$, which varies the prediction by 0.2 to 10%. To improve on the MADGRAPH modeling of the multiplicity of additional jets from initial state radiation (ISR), simulated signal events are reweighted based on the number of ISR jets (N_J^{ISR}) so as to make the jet multiplicity in MADGRAPH $t\bar{t}$ agree

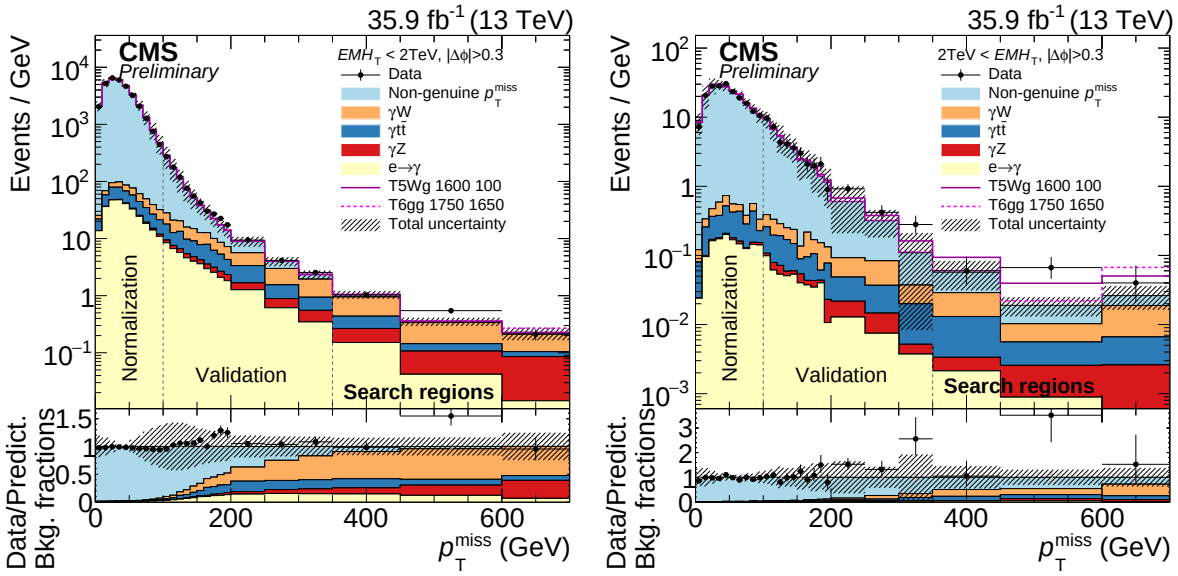

Figure 5: Observed data compared to the background prediction. Two signal models are shown added to the background. The expectation for the T5Wg signal scenario with a gluino mass of 1600 GeV and a gaugino mass of 100 GeV and the T6gg signal scenario with a squark mass of 1750 GeV and a neutralino mass of 1650 GeV are shown added to the background. The low-(high-)EMH_{T} selection is shown on the left (right). Below the $p_{\mathrm{T}}^{\mathrm{miss}}$ distributions, the data divided by the background prediction are shown as black dots, and the relative background components are shown as colored areas.

Table 1: Observed data compared to the background prediction and the expected signal yields for the T5Wg model with $m_{\tilde{g}} = 1600\,\mathrm{GeV}$ and $m_{gaugino} = 100\,\mathrm{GeV}$. The quadratic sum of statistical and systematical uncertainties are given. Only experimental uncertainties for the signal model are stated.

EMH_{T} (GeV)	< 2000			> 2000		
$p_{\mathrm{T}}^{\mathrm{miss}}$ (GeV)	(350,450)	(450,600)	(600,∞)	(350,450)	(450,600)	(600,∞)
Non-genuine $E_{\mathrm{T}}^{\mathrm{miss}}$	9.6 ± 11.1	2.2 ± 5.5	0.0 ± 0.0	2.83 ± 2.51	1.31 ± 0.74	0.73 ± 0.86
γW	51.3 ± 9.7	29.1 ± 5.5	11.6 ± 2.5	1.58 ± 0.58	0.70 ± 0.37	1.23 ± 0.43
$\gamma t\bar{t}$	17.1 ± 5.4	5.6 ± 2.6	1.9 ± 0.4	0.97 ± 0.38	0.45 ± 0.29	0.40 ± 0.22
γZ	11.5 ± 2.4	9.7 ± 1.8	7.1 ± 1.4	0.12 ± 0.07	0.25 ± 0.11	0.21 ± 0.10
$e \to \gamma$	15.1 ± 4.6	6.3 ± 1.9	1.4 ± 0.5	0.21 ± 0.10	0.13 ± 0.07	0.05 ± 0.04
Total	104.6 ± 16.5	53.0 ± 8.6	22.0 ± 3.0	5.72 ± 2.60	2.84 ± 0.89	2.62 ± 0.99
Data	103	82	21	6	10	4
Signal	0.4 ± 0.1	0.8 ± 0.1	0.7 ± 0.1	3.66 ± 0.40	3.09 ± 0.40	2.41 ± 0.32

with data. The reweighting factors vary between 0.92 and 0.51 for N_j^{ISR} between 1 and 6. We take one half of the deviation from unity as the systematic uncertainty on these reweighting factors.

The data in the search regions are interpreted in simplified models motivated by GMSB. These models are described in Section 3, and their corresponding Feynman diagrams can be seen in Fig. 1.

The 95% confidence level (CL) upper limits on the SUSY cross section are calculated using the asymptotic formulation of the LHC-style $\mathrm{CL_s}$ method [38–41]. Log-normal nuisance parameters are used to describe the systematic uncertainties. The observed cross section limits,

Table 2: Systematic uncertainties for data-driven backgrounds (first two rows) and simulation (all other rows). If two values are given, the first one is for SM simulation, while the latter is for signal simulation. The PDF and scale uncertainty for signal simulation is for the shape only, as the uncertainty on the rate is considered by [34].

Source	Relative uncertainty (%)
Non-genuine $p_{\mathrm{T}}^{\mathrm{miss}}$	14-100
$e \to \gamma$	30
Integrated Luminosity	2.6
Photon scale factors	2
Trigger	4
Jet energy scale and resolution	3–20 / 1–6
PDF	4–10 / 0
Renormalization and factorization scale	15–27 / 0–1
Pileup	0.2–6 / 2-10
ISR	0 / 0–10
FastSim $p_{\mathrm{T}}^{\mathrm{miss}}$ modelling	0 / 0.5–6

exclusion contours, and expected exclusion contours are shown in Fig. 6. More stringent limits can be set on models with two photons, since the probability that at least one photon is reconstructed is higher. The acceptance drops for low neutralino masses, since more energy is transfered to jets, leaving less energy available for the photon and the gravitinos and therefore resulting in a smaller $p_{\mathrm{T}}^{\mathrm{miss}}$. If the chargino mass is close to the W boson mass, less momentum is transfered to the gravitino, leading to smaller $p_{\mathrm{T}}^{\mathrm{miss}}$ values and therefore smaller sensitivity. Gluino masses up to 2 TeV and squark masses up to 1.6 TeV are excluded. For the squark pair production, the mass exclusion is determined assuming eight mass-degenerate squark states (partners of four flavors of quarks: u, d, c, s with two chirality states each).

We provide here the correlation matrix for our background predictions which can be used to aid in further interpretation of our search as outlined in Ref. [42].

7 Summary

A search for physics beyond the standard model in final states with at least one photon, transverse momentum imbalance, and total transverse event activity has been presented using data corresponding to an integrated luminosity of 35.9 fb^{-1} of proton-proton collisions recorded by the CMS experiment at the LHC in 2016. The SM background is estimated from data and simulation, and is validated in several control regions. No signs of new physics beyond the SM are found, and the data are interpreted in simplified models motivated by GMSB. Gluino masses up to 2 TeV and squark masses up to 1.6 TeV are excluded.

References

[1] R. Barbieri and G. F. Giudice, "Upper bounds on supersymmetric particle masses", *Nucl. Phys. B* **306** (1988) 63, doi:10.1016/0550-3213(88)90171-X.

[2] P. Ramond, "Dual theory for free fermions", *Phys. Rev. D* **3** (1971) 2415, doi:10.1103/PhysRevD.3.2415.

[3] Y. A. Gol'fand and E. P. Likhtman, "Extension of the algebra of Poincare group generators and violation of P invariance", *JETP Lett.* **13** (1971) 323.

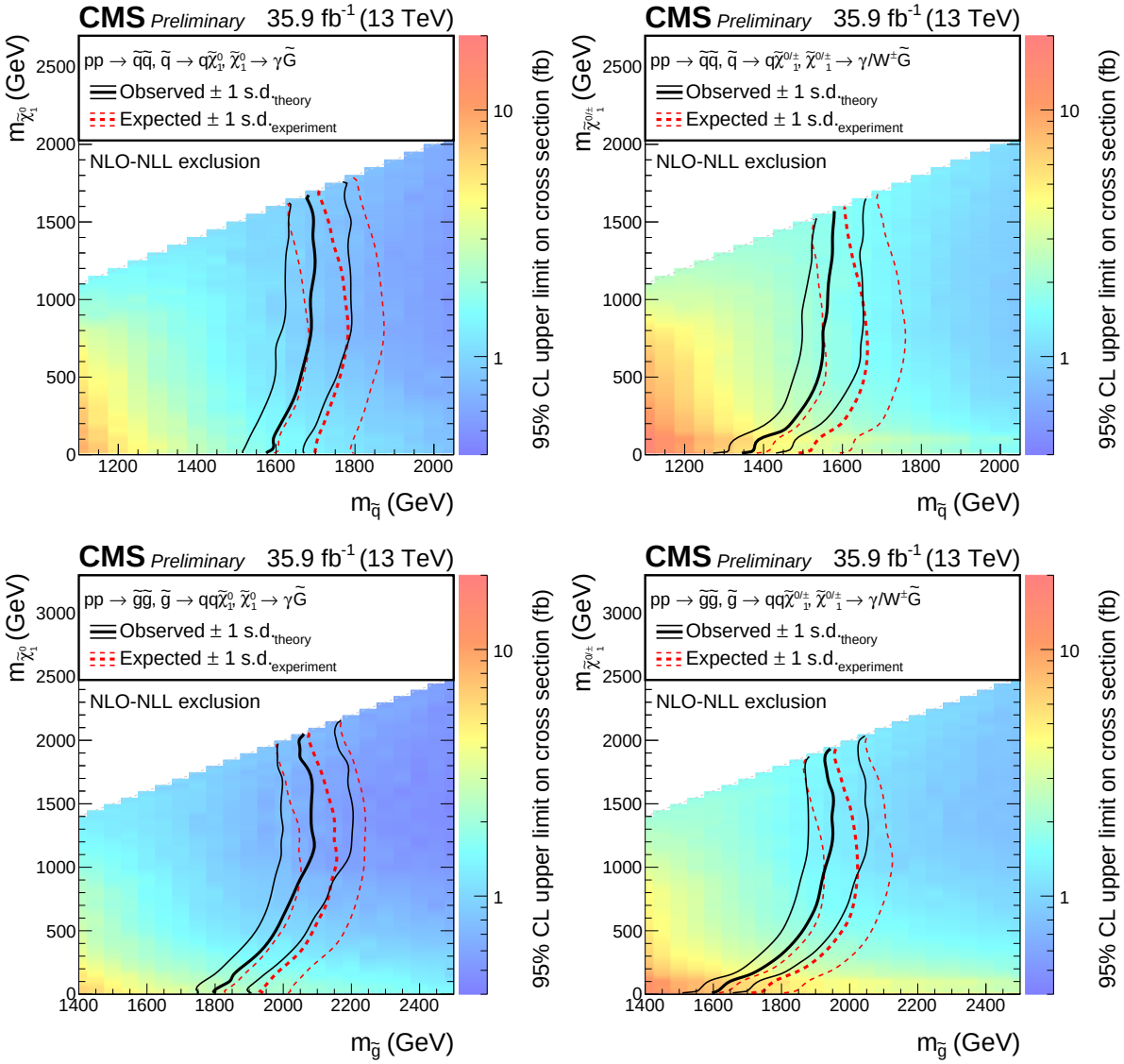

Figure 6: Exclusion limits at 95% CL for T6gg (top left) T6Wg (top right), T5gg (bottom left) and T5Wg (bottom right) models. The solid black curve represents the observed exclusion contour and the uncertainty due to the signal cross section. The red dashed curves represent the expected exclusion contours and the experimental uncertainties.

[4] S. Ferrara and B. Zumino, "Supergauge Invariant Yang-Mills Theories", *Nucl. Phys. B* **79** (1974) 413, doi:10.1016/0550-3213(74)90559-8.

[5] J. Wess and B. Zumino, "Supergauge transformations in four-dimensions", *Nucl. Phys. B* **70** (1974) 39, doi:10.1016/0550-3213(74)90355-1.

[6] A. H. Chamseddine, R. L. Arnowitt, and P. Nath, "Locally supersymmetric grand unification", *Phys. Rev. Lett.* **49** (1982) 970, doi:10.1103/PhysRevLett.49.970.

[7] R. Barbieri, S. Ferrara, and C. A. Savoy, "Gauge models with spontaneously broken local supersymmetry", *Phys. Lett. B* **119** (1982) 343, doi:10.1016/0370-2693(82)90685-2.

[8] L. J. Hall, J. D. Lykken, and S. Weinberg, "Supergravity as the messenger of supersymmetry breaking", *Phys. Rev. D* **27** (1983) 2359, doi:10.1103/PhysRevD.27.2359.

[9] P. Fayet, "Mixing between gravitational and weak interactions through the massive gravitino", *Phys. Lett. B* **70** (1977) 461, doi:10.1016/0370-2693(77)90414-2.

[10] H. Baer, M. Brhlik, C.-h. Chen, and X. Tata, "Signals for the minimal gauge-mediated supersymmetry breaking model at the Fermilab Tevatron collider", *Phys. Rev. D* **55** (1997) 4463, doi:10.1103/PhysRevD.55.4463, arXiv:hep-ph/9610358.

[11] H. Baer, P. G. Mercadante, X. Tata, and Y. Wang, "Reach of Fermilab Tevatron upgrades in gauge-mediated supersymmetry breaking models", *Phys. Rev. D* **60** (1999) 055001, doi:10.1103/PhysRevD.60.055001, arXiv:hep-ph/9903333.

[12] S. Dimopoulos, S. Thomas, and J. D. Wells, "Sparticle spectroscopy and electroweak symmetry breaking with gauge-mediated supersymmetry breaking", *Nucl. Phys. B* **488** (1997) 39, doi:10.1016/S0550-3213(97)00030-8, arXiv:hep-ph/9609434.

[13] J. Ellis, J. L. Lopez, and D. V. Nanopoulos, "Analysis of LEP constraints on supersymmetric models with a light gravitino", *Phys. Lett. B* **394** (1997) 354, doi:10.1016/S0370-2693(97)00019-1, arXiv:hep-ph/9610470.

[14] M. Dine, A. E. Nelson, Y. Nir, and Y. Shirman, "New tools for low energy dynamical supersymmetry breaking", *Phys. Rev. D* **53** (1996) 2658, doi:10.1103/PhysRevD.53.2658, arXiv:hep-ph/9507378.

[15] G. F. Giudice and R. Rattazzi, "Gauge-mediated supersymmetry breaking", in *Perspectives on Supersymmetry*, p. 355. World Scientific, Singapore, 1998.

[16] P. Grajek, A. Mariotti, and D. Redigolo, "Phenomenology of General Gauge Mediation in light of a 125 GeV Higgs", *JHEP* **07** (2013) 109, doi:10.1007/JHEP07(2013)109, arXiv:1303.0870.

[17] R. Barbier et al., "R-parity-violating supersymmetry", *Phys. Rep.* **420** (2005) 1, doi:10.1016/j.physrep.2005.08.006, arXiv:hep-ph/0406039.

[18] G. R. Farrar and P. Fayet, "Phenomenology of the production, decay, and detection of new hadronic states associated with supersymmetry", *Phys. Lett. B* **76** (1978) 575, doi:10.1016/0370-2693(78)90858-4.

[19] CMS Collaboration, "Search for supersymmetry with photons in pp collisions at $\sqrt{s} = 8$ TeV", *Phys. Rev. D* **92** (2015) 072006, doi:10.1103/PhysRevD.92.072006.

[20] ATLAS Collaboration, "Search for photonic signatures of gauge-mediated supersymmetry in 8 TeV pp collisions with the ATLAS detector", *Phys. Rev. D* **92** (2015) 072001, doi:10.1103/PhysRevD.92.072001, arXiv:1507.05493.

[21] ATLAS Collaboration, "Search for supersymmetry in a final state containing two photons and missing transverse momentum in $\sqrt{s} = 13$ TeV pp collisions at the LHC using the ATLAS detector", *Eur. Phys. J. C* **76** (2016) 517, doi:10.1140/epjc/s10052-016-4344-x, arXiv:1606.09150.

[22] CMS Collaboration, "Search for supersymmetry in electroweak production with photons and large missing transverse energy in pp collisions at sqrt(s) = 8 TeV", *Phys. Lett. B* **759** (2016) 479–500, doi:10.1016/j.physletb.2016.05.088, arXiv:1602.08772.

[23] CMS Collaboration, "Search for supersymmetry in events with photons and missing transverse energy in pp collisions at 13 TeV", *Submitted to: Phys. Lett. B* (2016) arXiv:1611.06604.

[24] CMS Collaboration, "Performance of photon reconstruction and identification with the CMS detector in proton-proton collisions at $\sqrt{s} = 8$ TeV", *J. Instrum.* **10** (2015) P08010, doi:10.1088/1748-0221/10/08/P08010.

[25] CMS Collaboration, "Jet energy scale and resolution in the CMS experiment in pp collisions at 8 TeV", *JINST* **12** (2017) P02014, doi:10.1088/1748-0221/12/02/P02014, arXiv:1607.03663.

[26] CMS Collaboration, "The CMS experiment at the CERN LHC", *JINST* **3** (2008) S08004, doi:10.1088/1748-0221/3/08/S08004.

[27] CMS Collaboration, "Particle–Flow Event Reconstruction in CMS and Performance for Jets, Taus, and $E_{\mathrm{T}}^{\mathrm{miss}}$", CMS Physics Analysis Summary CMS-PAS-PFT-09-001, 2009.

[28] CMS Collaboration, "Commissioning of the Particle-flow Event Reconstruction with the first LHC collisions recorded in the CMS detector", CMS Physics Analysis Summary CMS-PAS-PFT-10-001, 2010.

[29] M. Cacciari, G. P. Salam, and G. Soyez, "The anti-k_t jet clustering algorithm", *JHEP* **04** (2008) 063, doi:10.1088/1126-6708/2008/04/063, arXiv:0802.1189.

[30] M. Cacciari, G. P. Salam, and G. Soyez, "FastJet User Manual", *Eur. Phys. J. C* **72** (2012) 1896, doi:10.1140/epjc/s10052-012-1896-2, arXiv:1111.6097.

[31] J. Alwall et al., "The automated computation of tree-level and next-to-leading order differential cross sections, and their matching to parton shower simulations", *JHEP* **07** (2014) 079, doi:10.1007/JHEP07(2014)079, arXiv:1405.0301.

[32] NNPDF Collaboration, "Parton distributions for the LHC Run II", *JHEP* **04** (2015) 040, doi:10.1007/JHEP04(2015)040, arXiv:1410.8849.

[33] T. Sjostrand, S. Mrenna, and P. Z. Skands, "A Brief Introduction to PYTHIA 8.1", *Comput. Phys. Commun.* **178** (2008) 852, doi:10.1016/j.cpc.2008.01.036, arXiv:0710.3820.

[34] C. Borschensky et al., "Squark and gluino production cross sections in pp collisions at $\sqrt{s} = 13, 14, 33$ and 100 TeV", *Eur. Phys. J. C* **74** (2014) 3174, doi:10.1140/epjc/s10052-014-3174-y, arXiv:1407.5066.

[35] CMS Collaboration, "Interpretation of Searches for Supersymmetry with simplified Models", *Phys. Rev. D* **88** (2013) 052017, doi:10.1103/PhysRevD.88.052017, arXiv:1301.2175.

[36] GEANT4 Collaboration, "GEANT4: A Simulation toolkit", *Nucl. Instrum. Meth. A* **506** (2003) 250, doi:10.1016/S0168-9002(03)01368-8.

[37] CMS Collaboration, S. Sekmen, "Recent Developments in CMS Fast Simulation", in *Proceedings, 38th International Conference on High Energy Physics (ICHEP 2016): Chicago, IL, USA, August 3-10, 2016*. 2017. arXiv:1701.03850.

[38] A. L. Read, "Presentation of search results: the CL_s technique", *J. Phys. G* **28** (2002) 2693, doi:10.1088/0954-3899/28/10/313.

[39] T. Junk, "Confidence level computation for combining searches with small statistics", *Nucl. Instrum. Meth. A* **434** (1999) 435, doi:10.1016/S0168-9002(99)00498-2, arXiv:hep-ex/9902006.

[40] ATLAS Collaboration, CMS Collaboration, LHC Higgs Combination Group, "Procedure for the LHC Higgs boson search combination in Summer 2011", Technical Report CMS-NOTE-2011-005, ATL-PHYS-PUB-2011-11, CERN, Geneva, Aug, 2011.

[41] G. Cowan, K. Cranmer, E. Gross, and O. Vitells, "Asymptotic formulae for likelihood-based tests of new physics", *Eur. Phys. J. C* **71** (2011) 1554, doi:10.1140/epjc/s10052-011-1554-0, 10.1140/epjc/s10052-013-2501-z, arXiv:1007.1727. [Erratum: *Eur. Phys. J. C* **73** (2013) 2501].

[42] CMS Collaboration, "Simplified likelihood for the re-interpretation of public CMS results", Technical Report CMS-NOTE-2017-001, CERN, Geneva, Jan, 2017.